



Soft Matter

Magnetically driven in-plane modulation of the 3D orientation of vertical ferromagnetic flakes.

Journal:	<i>Soft Matter</i>
Manuscript ID	SM-ART-10-2021-001423.R2
Article Type:	Paper
Date Submitted by the Author:	23-Dec-2021
Complete List of Authors:	Le Ferrand, Hortense; Nanyang Technological University, Arrieta, Andres; Purdue University, Mechanical Engineering

SCHOLARONE™
Manuscripts

Research paper**Magnetically driven in-plane modulation of the 3D orientation of vertical ferromagnetic flakes.**

Hortense Le Ferrand^{1*}, Andres F. Arrieta²

¹H. Le Ferrand

School of Mechanical and Aerospace Engineering, 50 Nanyang Avenue, Nanyang Technological University, 639798 Singapore

²A. F. Arrieta

School of Mechanical Engineering, Purdue University, 585 Purdue Mall, West Lafayette, IN 47907, United States

E-mail: hortense@ntu.edu.sg

Keywords: magnetic fields, colloid orientation, 2D particles, microstructure, composite

Abstract

External magnetic fields are known to attract and orient magnetically responsive colloidal particles. In the case of 2D microplatelets, rotating magnetic fields are typically used to orient them parallel to each other in a brick-and-mortar fashion. Thanks to this microstructure, the resulting composites achieve enhanced mechanical and functional properties. However, parts with complex geometries require their

microstructure to be specifically tuned and controlled locally in 3D. Although the tunability of the microstructure along the vertical direction has already been demonstrated using magnetic orientation combined with sequential or continuous casting, controlling the particle orientation in the horizontal plane in a fast and effective fashion remains challenging. Here, we propose to use rotating magnetic arrays to control the in-plane orientation of ferromagnetic Nickel flakes distributed in curable polymeric matrices. We experimentally studied the orientation of the flakes in response to magnets rotating at various frequencies and precessing angles. Then, we used COMSOL to model the magnetic field from rotating magnetic arrays and predicted the resulting in-plane orientations. To validate the approach, we created composites with locally oriented flakes. This work could initiate reverse-engineering methods to design the microstructure in composite materials with intricate geometrical shapes for structural or functional applications.

1| Introduction

Submitting colloidal particles to external magnetic fields is of interest for studying interparticle interactions,¹ colloidal assembly and patterning,^{2,3} as well as for applications such as in medicine and robotics.⁴⁻⁶ More specifically to plate-like particles, also called microplatelets or flakes, controlling their orientation in polymeric matrices is one path to fabricating composites with enhanced mechanical properties and adding functionalities, such as complex shaping and morphing abilities.⁷⁻¹⁰ Ferromagnetic particles, such as from iron, cobalt, or nickel, can be oriented and arranged into chains depending on their concentration, the strength of the magnetic field applied, and their dipole-dipole interactions.^{11,12} Polymeric composites with anisotropic orientation of ferromagnetic particles were found to exhibit increased mechanical

properties, electrical and thermal conductivities along the reinforcement direction, as well as piezoresistivity, electromagnetic shielding, and transparency.^{13–16} Although homogeneously orientated composites have their advantage, locally controlling the microstructure over large areas in composites offer substantial potential for engineering hierarchical materials with local properties, for example for touch screens and smart sensors or actuators.^{17–19} Also, local microstructure in geometric shapes could help attaining unusual macroscopic properties, such as bioinspired complex crack paths,²⁰ auxeticity,²¹ or shape morphing.²² However, it remains challenging to purposely control the local orientation of 2D particles in 3D space in composite materials.

Plate-like microparticles are defined in space by two angles Φ_p and θ_p (**Figure 1A**). During composite forming, suspended magnetically-responsive microparticles with a sufficient magnetic susceptibility difference with the liquid polymeric matrix orient upon the application of a magnetic field.²³ In the case of ferromagnetic, paramagnetic or diamagnetic flakes, static magnetic fields control the angle θ_p (**Figure 1B**). To simultaneously set Φ_p and θ_p , magnetic fields rotating above a critical frequency have been applied on diamagnetic platelets coated with a ferromagnetic material (**Figure 1C**).^{24–26} These functionalized microplatelets do not generally exhibit any preferred direction of magnetization in-plane and have no remanent magnetization.²⁷ Magnetically responsive anisotropic particles of microscale dimensions tend to follow the directions of high magnetic fields strength to minimize their magnetic energy. As a result, the particles are found to rotate synchronously with the rotating magnetic field. When the rotation frequency of the magnetic field exceeds a critical value, the motion becomes asynchronous due to the unfavourable damping by the viscous drag. This transition from synchronous to asynchronous motion has been observed for paramagnetic, diamagnetic, and paramagnetic anisometric particles.^{28–30}

This results in particles aligning biaxially in the plane of rotation of the magnet.²⁴ The critical frequency ω_c of the magnetic field rotation depends on the anisotropy in magnetic susceptibility $\Delta\chi = \chi_{\parallel} - \chi_{\perp}$ of the particles, with χ_{\parallel} the susceptibility along the diameter and χ_{\perp} along the thickness, the viscosity η of the surrounding liquid, the magnetic field strength B_0 , and the Perrin friction factor $\frac{f}{f_0}$:³⁰

$$\omega_c = \frac{\Delta\chi \cdot B_0^2}{12 \cdot \eta \cdot \mu_0 \cdot \frac{f}{f_0}} \quad \text{(equation 1)}$$

1)

Using rotating permanent magnets, translating solenoids, or solenoids set-ups with on and off periodic control, magnetically responsive flakes have been oriented horizontally and biaxially in so-called brick-and-mortar arrangements ($\Phi_p = cst$ and $\theta_p = 0^\circ$ for all particles) as well as vertically and biaxially ($\Phi_p = cst$ and $\theta_p = 90^\circ$ for all particles) over large areas and in curable polymeric matrices.^{31,32} Indeed, when the magnet is rotating above the critical frequency ω_c , the microplatelets align in the plane of rotation of the magnet. If the magnet is rotating around a vertical axis, the microplatelets align horizontally. If the magnet is rotating around an axis in the horizontal plane, the microplatelets align vertically. Tuning the orientation of the rotating angle of the magnetic field at defined angles has been used to create similar biaxial orientations at set θ_p angles and fixed Φ_p (**Figure 1C**).³³ Such capability has been utilized to create multilayer composites with set angles θ_p in each layer.^{20,34} These materials are promising for mechanical dampening.³⁵ However, locally tuning the angles Φ_p within each layer using magnetic fields is still to be achieved. Realizing it would greatly enhance the geometric design capabilities of reinforced composites.

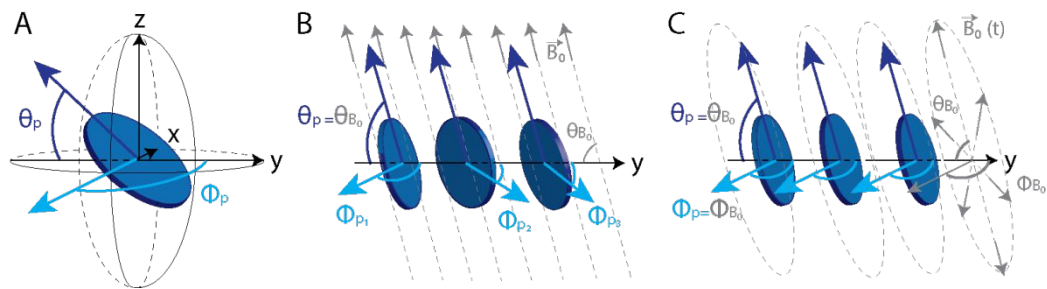


Figure 1: Orientation of magnetically responsive microparticles under magnetic fields. (A) Schematics representing a platelet described in the (x-y-z) frame by the two angles θ_p and Φ_p . (B) Schematics representing platelet orientation under static magnetic fields oriented at θ_{B_0} fixed. The resulting angles Φ_{p_i} vary for platelets $i = 1, 2, \dots$ (C) Schematics representing biaxial platelet orientation under magnetic fields rotating in a plane inclined at an angle θ_{B_0} and at an angle Φ_{B_0} in the (x-y) plane.

Several methods have been explored to realize in-plane modulation of the orientations of microplatelets in liquid matrices, such as acoustophoresis,³⁶ virtual magnetic molds,^{8,37,38} and combinations of 3D printing with magnetic fields.^{39,40} Acoustophoresis and virtual magnetic moulds use external acoustic pressure forces and magnetic attraction forces, respectively, to concentration and position the particles locally. However, they are not practical for the fabrication of composites materials as they require very low viscosity. 3D printing with magnetic fields consists in printing a liquid composition, placing the print under a rotating magnet for alignment, then curing before depositing the new layer. This method is timely and costly, especially for large surface areas. One alternative approach potentially reducing processing complexity could be to take advantage of the naturally-occurring modulations of the magnetic field distribution around permanent magnets of diverse shapes or arranged into arrays.^{41,42} It has been shown previously that magnetically responsive microplatelets could remain vertically orientated under a rotating magnet, while presenting curved orientations in

the horizontal plane in regions located at the edge of the magnet.⁴³ This feature has been used to tune the curvature of morphing composite bilayers with a leaf-shape geometry.^{43,44} Better control of the in-plane orientation of vertical particles (the angle Φ_p) could thus enable more complex composite morphing shapes, or allow geometrical designs with specific, local reinforcement.

In this paper, we explored the orientation control of ferromagnetic nickel flakes experimentally and carry out simple simulations to predict their orientations in selected patterns. The orientation of the Ni flakes was achieved in liquid polymeric matrices which were turned into a composite after curing. First, we observed the response of the ferromagnetic flakes under vertically rotating magnetic fields. Then, we characterized their response under fields rotating at various precessing angles. Using theoretical and experimental results, we simulated the field lines around the magnets to predict the platelets orientations in the horizontal plane and verified our predictions with magnets of simple geometries. Finally, we built arrays of magnets to achieve unusual radial and circular in-plane orientations of vertical Ni flakes. The results presented show a simple and scalable approach to set the in-plane orientations of vertical ferromagnetic flakes in composites. Such in-plane local variations of the microstructure could enable more geometrical design capabilities. This could be used to create materials adapted to complex external loadings, or with complex deformations or functional response for smart applications using a reverse engineering approach (**Figure 2**).

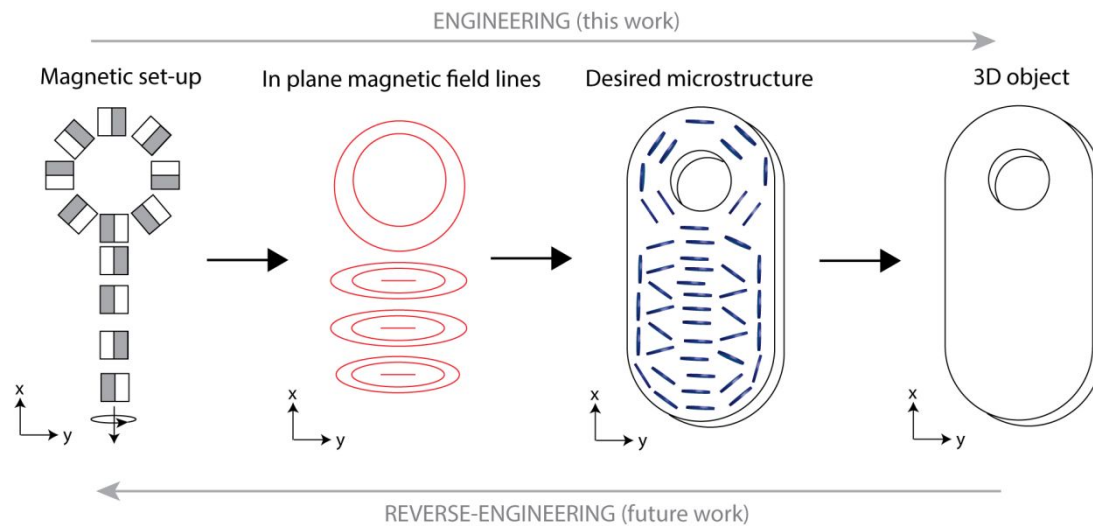


Figure 2: Schematic of the engineering approach for engineering microstructured materials and its potential for future reverse-engineering.

2| Experimental

2.1| Materials

Nickel flakes (fine leafing) of diameter $15.8 \pm 0.7 \mu\text{m}$ and thickness $0.58 \pm 0.01 \mu\text{m}$ were obtained from Novamet, USA. These flakes have non-uniform shapes and an average aspect ratio length over thickness of 27 (**Figure 3**). The flakes did not exhibit any preferred direction of magnetization and had a remanent magnetization of $16 \times 10^{-6} \text{ Am}^2/\text{kg}$, according to the manufacturer. The size distributions were obtained from electron micrographs and analysed using Image J and MATLAB. Epoxy was obtained from Hunstmann, Belgium: resin Araldite GY250, hardener Aradur 917 CH and catalyst DY070. Polydimethylsiloxane (PDMS), Sylgard 184 was purchased from Dow Chemicals, USA. Neodymium magnets were used purchased from Supermagnete, Switzerland.

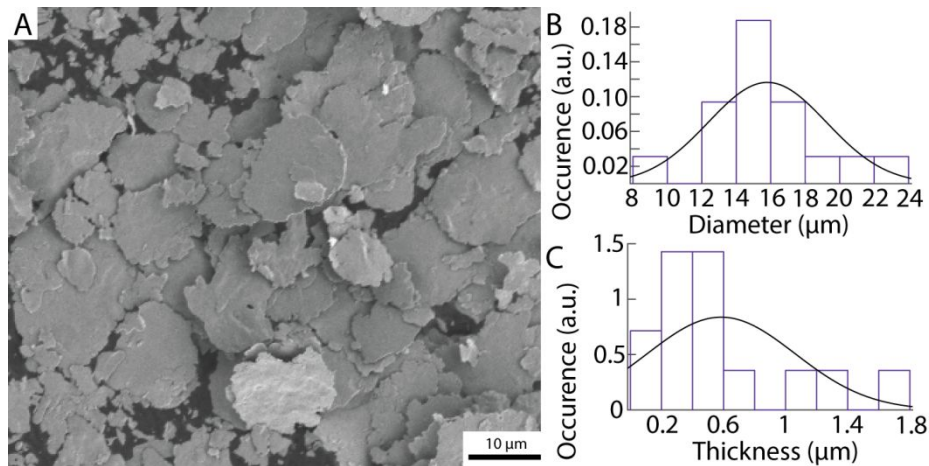


Figure 3: (A) Electron micrograph of the Ni flakes. (B) and (C) are the distributions of flakes diameters and thicknesses, respectively.

2.2| Nickel-epoxy composites preparation.

Nickel-epoxy composites were prepared by dispersing 1 vol% of nickel flakes into the epoxy mixture containing 53.5 wt% of the resin, 45.7 wt% of the hardener and 0.8 wt% of the catalyst. The mixture was mixed with an overhead stirrer until homogeneous and degassed under vacuum. The casting was done in a Teflon mould placed over a non-magnetic hot plate set at 180 °C for 4 hours to cure the composite during the magnetic alignment.

2.3| Nickel-PDMS composites preparation.

Nickel-PDMS composites were prepared by mixing the PDMS solution at a ratio resin to hardener of 10 to 1 and adding 0.01 vol% of Nickel flakes. A low concentration in Ni powder was used to retain the transparency of the composites after curing. The Ni-PDMS mixture was spread onto an aluminium block and placed under the magnetic setup and above a non-magnetic hot plate set at 120°C for 30 minutes to cure the matrix. For the Ni-PDMS composites used for the determination of the critical frequency, no temperature was applied to avoid curing and to maintain the viscosity constant.

2.4| Magnetic setups.

For the magnetically oriented epoxy specimens, the magnet used had dimensions of $5*5*1.5\text{ cm}^3$ and was placed at around 10 cm from the top of the sample. This led to a magnetic field strength at the position of the sample of around 3 mT. A rotating magnetic field was achieved by attaching the magnet to a stirrer rotating at a frequency above 1 Hz. The large size of the magnet was used to generate particle orientation over a large area. The magnetic field was maintained during the entire curing time of the samples. For the magnetically oriented PDMS specimens, the utilized magnets had smaller dimensions of $0.5*0.5*0.5\text{ cm}^3$ to allow their assembly into various arrays. The magnets were mounted onto other stirrers in similar configurations during the entire curing of the composite, at 1.5 cm to the surface of the sample. The magnetic field strength at the position of the sample was also of around 3 mT.

2.5| Characterization methods.

Electron micrographs of the raw powder and of the cross-sections of epoxy composites were taken using a scanning electron microscope (Leo 1530, Zeiss, Germany), after sputtering with Pt. The epoxy composites were brittle and could be fractured for the direct observation of the cross-section. For observations in the plane, the samples were polished using sandpaper. The orientation angles of the flakes were measured using the Image J software (NIH, USA). The PDMS composites were observed by optical methods thanks to their transparency using a common digital camera. The critical alignment frequencies under magnets rotating with precessing angles were assessed by recording videos of the mixture under the alignment setup. When the flakes are rotating, a colour change could be seen at the surface of the sample, accompanied by waves (see

SI movie S1). Flakes rotating asynchronously with the rotating magnetic fields appear to be still at the surface of the sample (see **SI movie S2**). The determination of the critical frequencies was done by increasing the frequency every 5 minutes until no more surface change was visible. Indeed, the expected time to have alignment of the nickel flakes under 3 mT was calculated to be of 3.3 s for the epoxy matrix and of 0.9 s for the PDMS using the following equation and the values in **Table 1**:

$$t = \frac{9\pi^2 \cdot \frac{f}{f_0} \eta (\chi_{ps} + 1)}{\mu_0 \chi_{ps}^2 B_0^2}, \quad \text{(equation 2)}$$

with μ_0 the magnetic susceptibility of vacuum, $\frac{f}{f_0}$ the Perrin friction factor, χ_{ps} the magnetic susceptibility of the particles.³⁹

Table 1: Values of experimental parameters.

Parameter	Symbol	Value	Unit
Flake diameter	$2 \cdot b$	15.8	μm
Flake thickness	$2 \cdot a$	0.58	μm
Aspect ratio	p	27	-
Perrin friction factor	$\frac{f}{f_0}$	12.1	-
Magnetic field strength	B_0	3	mT
Magnetic susceptibility	χ_{ps}	600	-
Viscosity (epoxy)	η	13.3	kg/m.s
Viscosity (PDMS)	η	3.5	kg/m.s

2.6| Simulations.

Magnetic fields around permanent magnets were simulated using COMSOL Multiphysics, Version 4.4. The geometries of the magnets were drawn, and the neodymium material was added to the materials library using a relative permeability of

1.05. The material around the magnet was set as air (relative permeability of 1). The magnetic fields were computed using the AC/DC module with magnetic fields, no currents interface. The boundary conditions were set such as:

- The magnetic field was tangential to the boundary on planes of symmetry.
- The magnetic field was perpendicular to the boundary on planes of antisymmetry.

The magnetic field at the surface of the magnet was set at a value of 250 mT measured at the surface of the magnets. The simulation yields the magnetic flux density vectors and streamlines as output, which were plotted in 3D around static permanent magnets. To obtain the projection of the field lines in sample located in a plane at a distance d to the magnet, the field was averaged over time at a given position over one rotation.

3| Results and discussion

3.1| Response of Ni flakes under vertically rotating magnetic fields ($\theta_{B_0} = 90^\circ$, Φ_{B_0} variable) and ($\theta_{B_0} = 90^\circ$, $\Phi_{B_0} = cst$).

Although rotating magnetic fields have been largely applied to orient magnetically responsive para or diamagnetic anisotropic platelets,^{24–26,31,45} the response of ferromagnetic flakes to dynamic fields has been overlooked. Therefore, the response of Ni flakes to vertical static and rotating magnetic fields was first observed in epoxy composites containing ca. 1 vol% of flakes (**Figure 4**).

The magnetic fields strength applied were low, below 3 mT, to avoid the formation of large magnetic gradients and the attraction of the Ni flakes to the magnet. Under static vertical magnetic fields ($\theta_{B_0} = 90^\circ$), the Ni flakes align uniaxially ($\theta_p = 90^\circ$, variable Φ_p) (**Figure 4A**). To determine the critical frequency ω_c of the rotating field to obtain vertical biaxial alignment of the flakes ($\theta_p = 90^\circ$, $\Phi_p = cst$ for all particles), a torque

balance equation between the magnetic, gravitational, and viscous torques has to be solved.²⁴ The critical frequency ω_c was then estimated using the values presented in

Table 1 and the following formula:²⁴

$$\omega_c = \frac{\mu_0 \chi_{ps}^2 B_0^2}{18 \frac{f}{f_0} \eta (\chi_{ps} + 1)^2} \quad \text{(equation 3)}$$

with μ_0 the magnetic susceptibility of vacuum, $\frac{f}{f_0}$ the Perrin friction factor, χ_{ps} the magnetic susceptibility of the particles, and B_0 the magnetic field strength. With this approximation, a critical frequency of 0.23 Hz was determined for our epoxy matrix, and of 0.9 Hz for PDMS. Applying a vertical magnetic field ($\theta_{B_0} = 90^\circ$, $\Phi_{B_0} = 90^\circ$) rotating above 1 Hz, vertical biaxial orientation of the flakes was also observed ($\theta_p = 90^\circ$, $\Phi_p = 90^\circ$) (**Figure 4B**). However, in contrast to superparamagnetic platelets, the ferromagnetic flakes used in this study also formed long chains that oriented along the field lines ($\Phi_p = 90^\circ$) due to their dipole-dipole interactions.^{12,46} We could observe this chain formation optically in dilute Ni-PDMS transparent films. Chain formation is ubiquitous for ferromagnetic powders exposed to magnetic fields and depends upon filler concentration and magnetic field.¹¹ The absence of clear chain formation under static magnetic fields might be related to the high viscosity of the matrix and its curing, which did not allow sufficient time for the flakes to translate and self-assemble. However, under rotating fields the flakes rotate and can act as local micromixers, reducing the local viscosity of the matrix when they have shear-thinning properties like here.⁴⁷ Also, the rotation of the flakes in the (x - y) plane (angle Φ_p) made the observation more difficult since the chains would have formed along the vertical direction.

In addition to the orientation of the flakes under the vertical magnets, we inspected the flake orientations variation along the axis y , where $y = 0$ corresponds to the center of the rotating magnet (**Figure 4C**). The angles θ_p of the flakes decreased as y increased

until the edge of the magnet at $y = 2.5$ cm. The flakes are thus sensitive to the field streamlines orientations.

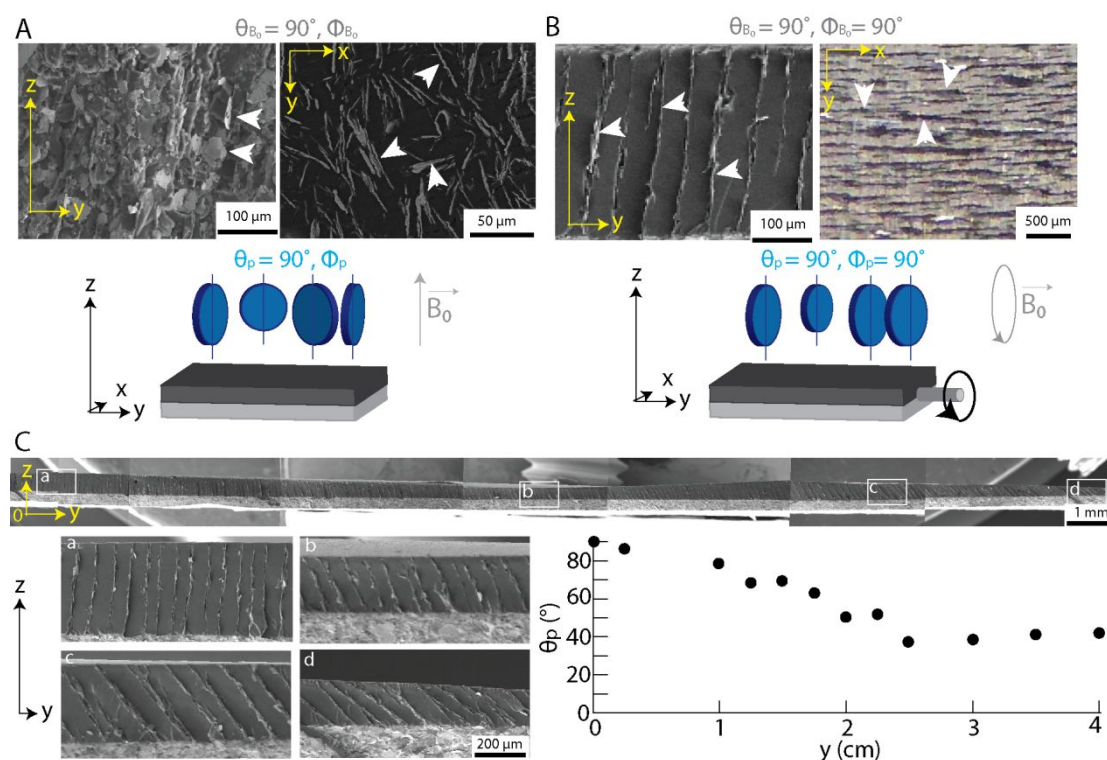


Figure 4: Response of Ni flakes to vertical magnetic fields. (A) Electron micrographs of Ni-epoxy composites showing uniaxial orientation under static vertical magnetic field. The white arrows indicate some Ni flakes. **(B)** Micrograph (left) and optical image (right) of epoxy and PDMS composites, respectively, showing biaxial orientation and chain formation of the Ni flakes under rotating vertical magnetic field. **(C)** Juxtaposed micrographs of the cross section of a large epoxy composite prepared under rotating vertical magnetic field ($\theta_{B_0} = 90^\circ$, $\Phi_{B_0} = 90^\circ$) centered at $x = 0$ and $y = 0$. Inserts are close-up view. Graph of the particle angle θ_p as a function of their position along y for $x = 0$.

3.2| Response of Ni flakes under magnetic fields rotating with a precessing angle ($\theta_{B_0} = 90^\circ - \alpha$, $\Phi_{B_0} = cst$).

To further study the response of the Ni flakes to rotating magnetic fields, a precessing angle α was added to the rotating magnet. The in-plane orientations of the flakes Φ_p in transparent PDMS composites were characterized optically (**Figure 5**). In this configuration, the magnetic field rotates at angles $\theta_{B_0} = 90^\circ - \alpha$ (**Figure 5A**). Previous works on ellipsoid magnetic particles under precessing magnetic fields have reported that biaxial alignment could also be achieved, at a critical frequency that decreased with the precessing angle.³⁰ Recording videos of the liquid PDMS-Ni mixtures under the precessing magnetic fields, the critical frequency for the alignment could be determined by optical visualization. The experimental results show good agreement with the expected prediction from ref³⁰, with the observation of an asynchronous regime where the particles align biaxially above a set frequency that decreases with the precessing angle (**Figure 5B,C**). The critical frequency was almost multiplied by 3 at low angles. This is higher than what has been reported elsewhere, where the frequency doubled only.³⁰ One reason could be that by tilting the magnet without moving its rotation axis or the sample, the magnetic field at the place of observation also increases because the edge of the magnet comes closer to the surface of the sample. Indeed, the magnetic field strength is usually higher at the edge of the magnets. A high magnetic field strength leads to a higher magnetic response of the particles.

The response of Ni flakes to magnetic fields rotating around a horizontal axis above the sample, and with a precessing angle was thus vertical orientation and biaxial alignment ($\theta_p = 90^\circ$, $\Phi_p = 90^\circ$) for all precessing angles except 90° (**Figure 5D**). The flakes aligned in the plane along the field lines of the magnet. At $\alpha = 90^\circ$, the magnetic field is horizontal at the position of the sample, below the magnet. This resulted in an increase in transparency of the composite sample and the absence of visible chains

(**Figure 5E**). This visual appearance was attributed to the horizontal orientation of the flakes in the plane. Indeed, the field lines are rotating in-plane.

Under rotating vertical magnetic fields, the ferromagnetic flakes align parallel to the plane of rotation described by the magnetic field. To obtain various orientations Φ_{pi} , with i each individual flake, within the (x-y) plane of the sample, it is therefore necessary to have rotating magnetic fields with locally oriented field lines.

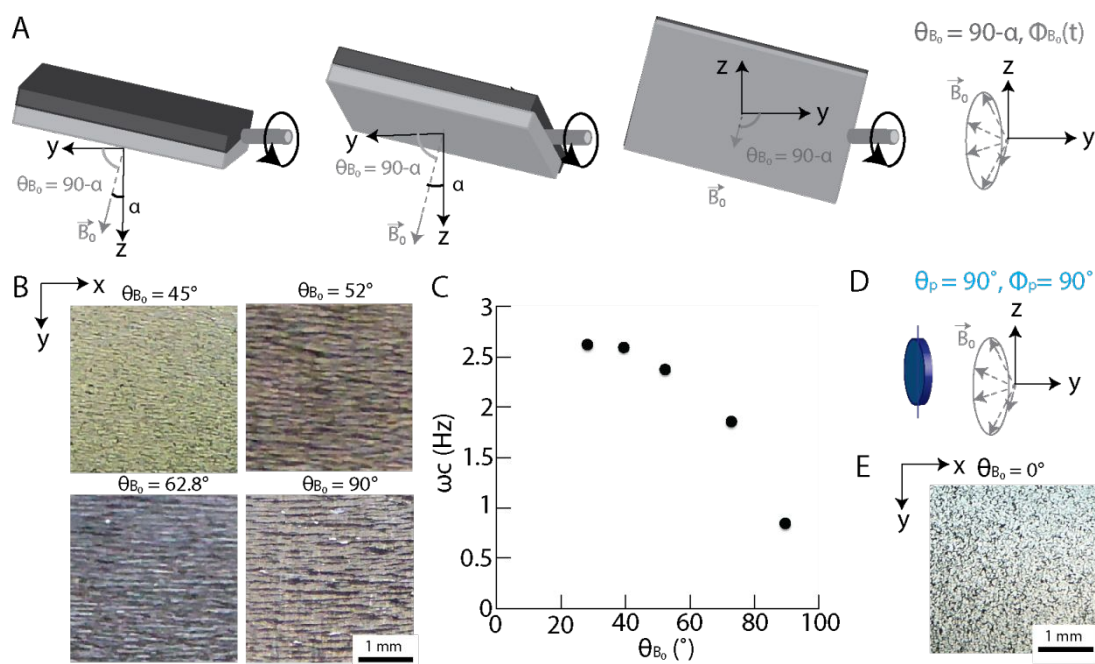


Figure 5: Nickel flake response to precessing vertical magnetic fields. (A) Schematics for a magnet rotating with a precessing angle α . **(B)** Optical images in the (x-y) plane of the sample centred below the magnet showing the line formation and alignment of the Ni flakes within the PDMS matrix. **(C)** Critical frequency as a function of the magnetic field angle θ_{B_0} . **(D)** Schematics of the flake orientation with the rotating magnetic field. **(E)** Optical image of the Ni-PDMS composite sample under a precessing angle $\alpha = 90^\circ$ ($\theta_{B_0} = 0$).

3.3| In-plane modulation of Ni flakes orientation under rotating magnets ($\theta_{B_0} = 90^\circ$, $\Phi_{B_0} =$ locally varying).

To modulate the in-plane angle of the vertically oriented flakes, we looked at their orientation away from the centre of the magnet, where the field lines are curved. First, we selected a cubic and a spherical magnet and used COMSOL to obtain the magnetic streamlines around the magnets. Then, we averaged the field over time at a given position over one rotation to obtain the map of Φ_{B_0} in the (x-y) plane of the sample (**Figure 6**). The vertical orientation of the flakes is assured by having the magnet positioned above the sample and rotating around a horizontal axis. Ni-PDMS composites were then prepared under the same magnetic setups rotating at a frequency higher than 3 Hz to ensure the asynchronous biaxial alignment of the Ni flakes (**Figure 6A,B**). The experimental specimen exhibited similar flake orientations as predicted by the simple model, showing flakes that are vertical, but oriented in-plane along curved lines. Magnetic field gradients in the sample due to variations in local magnetic field strengths also gave rise to variations in flakes concentration. Although the model is simplistic and its resolution is not yet high enough to match the exact orientation at the microscale, it gives a qualitative view of the expected orientations of vertical flakes in-plane across areas of a few millimetres to centimetres.

We applied this approach to generate more complex patterns of vertical flakes orientation in plane, using magnetic arrays made from assemblies of magnets (**Figure 7**). Small cubic permanent magnets were assembled to generate more complex magnetic streamlines. The assembly of the magnets was inspired from that of Halbach arrays and others. The intention was to obtain unusual flake orientation in-plane, such as radial and circular (**Figure 7A,B**), extended to large areas (**Figure 7C**), and with local patterns (**Figure 7D, E**). For each magnet assembly, the magnetic streamlines

were simulated. Then the magnetic assemblies were rotated along a horizontal axis above the sample. The flakes oriented during the curing of the matrix. After curing, optical imaging was used to determine the in-plane orientation of the flakes. The flakes in plane orientation corresponded to the expectations from the streamlines, although there were local variations in concentrations.

A more refined model of the rotating magnetic fields and of the flakes' response to these fields would push the approach proposed here to a next level. For this, modelling based on the constitutive equations of magnetic fields and with finite element modelling methods could be envisaged.^{48,49} With such accurate modelling schemes, reverse engineering of flake orientations in 3D might be realized. The modelling could also include concentration gradients. Reverse-engineering could work in the following way: first, for a given in-plane desired alignment pattern, a magnetic field will be derived. The magnetic field will then be approximated by combinations of magnets or magnets with complex shapes. Then, the magnetic field will be averaged over time to visualize the in-plane orientation map. Finally, the prediction will be applied in experiments using the set magnetic set-up.

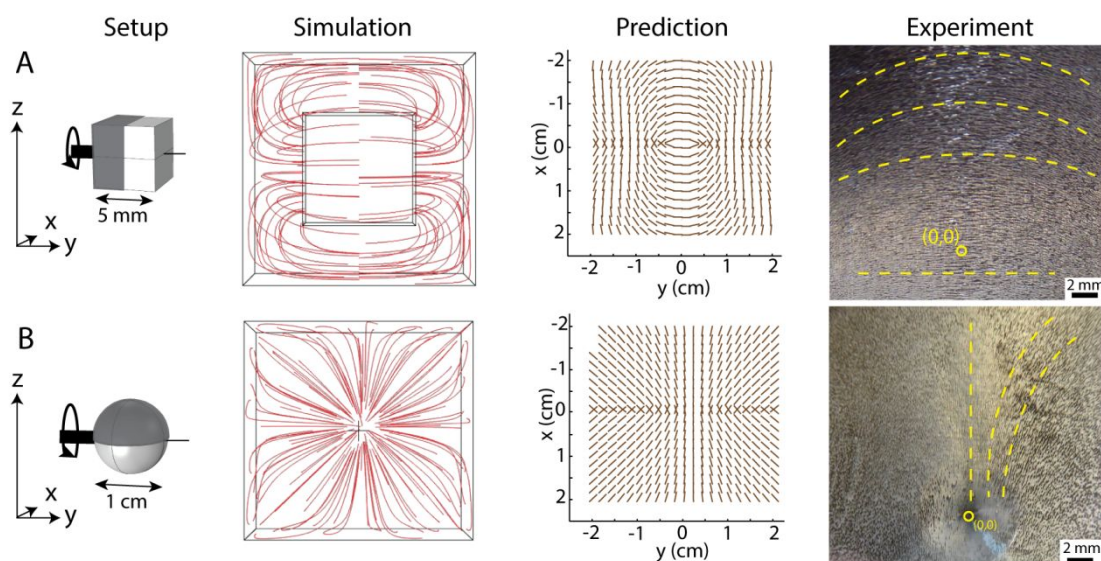


Figure 6: Predicting the in-plane modulation of Ni flakes orientation under vertical rotating cubic (A) and spherical (B) magnets. Setup, simulation, prediction, and experiment flow to predict and realize in-plane modulation of the Φ_p . The axis of rotation of the magnets is highlighted in bold and the north and south pole in dark and light grey colour, respectively. The red lines around the magnets are the simulated magnetic streamlines, top view in (x-y) plane. The lines in the x-y plot are tilted at the local angles Φ_p of the flakes. The experimental images are pictures of Ni-PDMS transparent samples after curing. The yellow lines are guides to the eye.

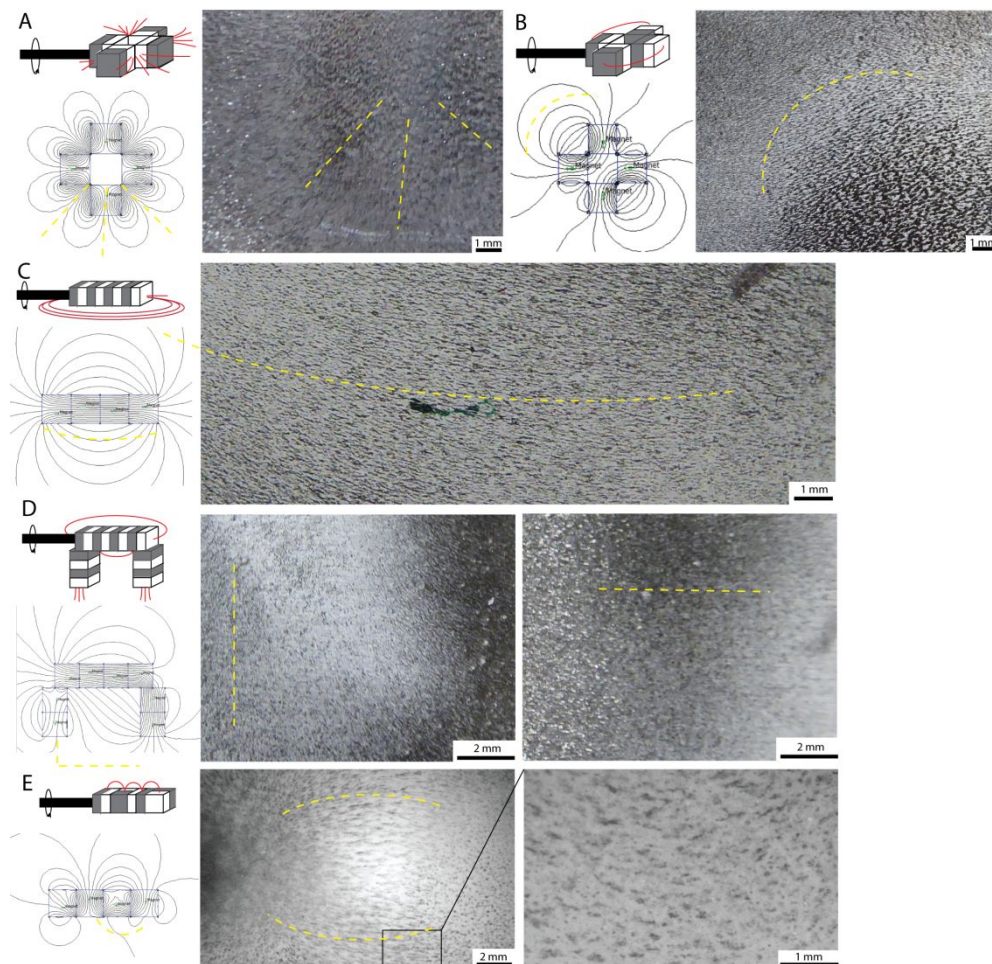


Figure 7: Alignment patterns obtained using rotating magnet arrays: (A) radial, **(B)** circular, **(C)** aligned, **(D)** combination of two perpendicular directions, and **(E)** locally curved orientations. The yellow lines highlight the flakes orientation in plane.

4| Conclusions and outlook

In this paper, we presented a practical approach to modulate the in-plane orientation of vertically oriented ferromagnetic Nickel flakes in polymer composites. The approach consists of distributing the flakes in uncured viscous polymeric matrices and to rotate arrays of magnets above the mixture while it is curing. The time for magnetic orientation depends on the flakes magnetic properties, the magnetic field strength, and the viscosity of the matrix, and typically varies from a few seconds to a few minutes.^{31,50} The curing method can thus be chosen accordingly to allow sufficient time for the magnetic orientation. After curing, the flakes retain their orientation. We also show that the in-plane orientation can be designed from the rotating magnetic field streamlines. This feature is key to further develop a reverse-engineering approach to design complex in-plane orientations in composites according to geometrical, structural, or functional demands, using methods such as finite element modelling, artificial intelligence or machine learning.^{51,52}

Along with the modulation in plane of the orientation of the flakes, a similar approach could be used to vary the local concentration in magnetic flakes. Indeed, gradients in magnetic field strengths can generate attractive forces on ferromagnetic flakes and concentrate them at the areas of strongest magnetic fields. This principle is called magnetophoresis and is well established.⁵³ Particles with strong magnetic susceptibility would respond faster to gradients in magnetic field, whereas particles with weaker magnetic susceptibility would be less sensitive to these gradients, in the limit that these particles still orient with the magnetic field.

Since the mechanism behind the assembly under the magnetic fields result from a torque balance between magnetic, viscous, and gravitational torque, paramagnetic or

diamagnetic particles could be assembled along a similar scheme. Owing to the lower magnetic susceptibilities of such particles, the magnetophoresis effect could be reduced while retaining orientation control. Also, the use of such magnet would reduce the chain formation and yield a homogeneous distribution of particles through-out the composite, as reported in the literature.^{32,54,55} In the future, combining the control of the local flake orientation with the control of the local magnetic concentration in composites would provide a large degree of design freedom. This freedom in design is particularly interesting for the fabrication of reinforced composites with complex geometries or submitted to complex loadings.

Concrete illustrative applications of this design capability can thus be found in the field of bioinspired reinforced composites. Similarly to bones where minerals are oriented and concentrated along load-bearing directions,^{56–58} bioinspired reinforced composites could have their internal microstructure set to reinforce specific loading directions. Another promising application is for the fabrication of shape-adaptable and magnetically actuated materials for robotics or medicine.^{59–61} Although such materials can be produced using microfibers oriented during 3D printing, employing flakes instead of fibers would increase the possible morphing designs.^{62,63} However, 3D printing with magnetically oriented flakes is still time-consuming because each little voxel printed has to be oriented independently before printing the next voxel.^{39,64} The method proposed here, where the in-plane orientation of the flakes is controlled locally over large area could provide an alternative facile, efficient, and scalable method. To this aim, it might be required to build complex magnetic arrays and set-ups. The recent developments in 3D printing of magnets could help in generating the desired magnetic fields patterns.^{66–68}

Associated content

Movie S1

Ni-PDMS composite under a rotating magnetic precessing at an angle of $\theta_{B_0} = 45^\circ$ and a frequency of 0.8 Hz, below the critical frequency for biaxial alignment.

Movie S2

Ni-PDMS composite under a rotating magnetic precessing at an angle of $\theta_{B_0} = 45^\circ$ and a frequency of 3.2 Hz, above the critical frequency for biaxial alignment.

Notes

The authors declare no competing financial interest.

Acknowledgements

The authors acknowledge financial support from the Ministry of Education, Singapore under Grant No. 2019-T1-001-002. Xin Ying Chan is thanked for simulating the magnetic fields emanating from the magnetic assemblies and for repeating the experiments.

References

1. Dagallier, C., Cardinaux, F., Dietsch, H. & Scheffold, F. Magnetic orientation of soft particles in a jammed solid. *Soft Matter* **8**, 4067–4071 (2012).
2. Kamal, M. A., Petukhov, A. V. & Pal, A. Path-Dependent Self-Assembly of Magnetic Anisotropic Colloidal Peanuts. *J. Phys. Chem. B* **124**, 5754–5760 (2020).
3. Bharti, B., Kogler, F., Hall, C. K., Klapp, S. H. L. & Velez, O. D. Multidirectional colloidal assembly in concurrent electric and magnetic fields.

- Soft Matter* **12**, 7747–7758 (2016).
4. Löwen, H. Colloidal soft matter under external control. *J. Phys. Condens. Matter* **13**, 415–432 (2001).
 5. Heinrich, D. *et al.* Effects of magnetic field gradients on the aggregation dynamics of colloidal magnetic nanoparticles. *Soft Matter* **11**, 7606–7616 (2015).
 6. Zhang, J. *et al.* Liquid Crystal Elastomer-Based Magnetic Composite Films for Reconfigurable Shape-Morphing Soft Miniature Machines. *Adv. Mater.* **33**, 1–9 (2021).
 7. Lin, Z. *et al.* Magnetic alignment of hexagonal boron nitride platelets in polymer matrix: Toward high performance anisotropic polymer composites for electronic encapsulation. *ACS Appl. Mater. Interfaces* **5**, 7633–7640 (2013).
 8. Le Ferrand, H. *et al.* Magnetic assembly of transparent and conducting graphene-based functional composites. *Nat. Commun.* **7**, 1–9 (2016).
 9. Le Ferrand, H. Magnetic slip casting for dense and textured ceramics: A review of current achievements and issues. *J. Eur. Ceram. Soc.* **41**, 24–37 (2021).
 10. Le Ferrand, H., Studart, A. R. & Arrieta, A. F. Filtered Mechanosensing Using Snapping Composites with Embedded Mechano-Electrical Transduction. *ACS Nano* **13**, 4752–4760 (2019).
 11. Borin, D. Targeted patterning of magnetic microparticles in a polymer composite. *Philos. Trans. R. Soc. A Math. Phys. Eng. Sci.* **378**, 2–16 (2020).
 12. Jang, S. H., Park, Y. L. & Yin, H. Influence of coalescence on the anisotropic mechanical and electrical properties of nickel powder/polydimethylsiloxane composites. *Materials (Basel)*. **9**, 1–11 (2016).
 13. Chen, Y. *et al.* Large-scale R2R fabrication of piezoresistive films (Ni/PDMS)

- with enhanced through thickness electrical and thermal properties by applying a magnetic field. *RSC Adv.* **5**, 92071–92079 (2015).
14. Park, K., Jin, S. & Kim, G. Transparent window film with embedded nano-shades for thermoregulation. *Constr. Build. Mater.* **269**, 121280 (2021).
 15. Göktürk, H. S., Fiske, T. J. & Kalyon, D. M. Effects of particle shape and size distributions on the electrical and magnetic properties of nickel/polyethylene composites. *J. Appl. Polym. Sci.* **50**, 1891–1901 (1993).
 16. Sancaktar, E. & Dilsiz, N. Anisotropic alignment of nickel particles in a magnetic field for electronically conductive adhesives applications. *J. Adhes. Sci. Technol.* **11**, 155–166 (1997).
 17. Stassi, S. *et al.* Smart piezoresistive tunnelling composite for flexible robotic sensing skin. *Smart Mater. Struct.* **22**, 125039 (2013).
 18. Kedambaimoole, V. *et al.* PDMS encapsulated graphene-nickel composite film as flexible tactile sensor. *Proc. IEEE Sensors 2017-Decem*, 1–3 (2017).
 19. Niu, S. *et al.* Tunable piezoresistivity of low percolation threshold micro-nickel wires/PDMS conductive composite regulated by magnetic field. *J. Mater. Chem. C* **9**, 5908–5919 (2021).
 20. Le Ferrand, H., Bouville, F., Niebel, T. P. & Studart, A. R. Magnetically assisted slip casting of bioinspired heterogeneous composites. *Nat. Mater.* **14**, 1172–1179 (2015).
 21. Zheng, G. Q. *et al.* Spin-echo NMR in pulsed high magnetic fields up to 48 T. *J. Phys. Soc. Japan* **78**, 274–292 (2009).
 22. Erb, R. M., Sander, J. S., Grisch, R. & Studart, A. R. Self-shaping composites with programmable bioinspired microstructures. *Nat. Commun.* **4**, 1–8 (2013).
 23. Coey, J. M. D. *Magnetism and Magnetic Materials*. (Cambridge University

- Press, 2010). doi:DOI: 10.1017/CBO9780511845000.
24. Erb, R. M., Segmehl, J., Charilaou, M., Löffler, J. F. & Studart, A. R. Non-linear alignment dynamics in suspensions of platelets under rotating magnetic fields. *Soft Matter* **8**, 7604–7609 (2012).
 25. Liu, C., Cai, J., Gong, D., Zhang, W. & Zhang, D. Fabrication and uniform alignment of nickel-coated diatomite flakes by rotating magnetic fields. *J. Magn. Magn. Mater.* **484**, 472–477 (2019).
 26. Lin, F., Niu, C., Hu, J., Wang, Z. & Bao, J. Graphene Diamagnetism. Levitation, transport, rotation, and orientation alignment of graphene flakes in a magnetic field. *IEEE Nanotechnol. Mag.* **1**, 14–22 (2020).
 27. Niebel, T. P. *et al.* Multifunctional microparticles with uniform magnetic coatings and tunable surface chemistry. *RSC Adv.* **4**, 62483–62491 (2014).
 28. Gu, Y. & Kornev, K. G. Ferromagnetic Nanorods in Applications to Control of the In-Plane Anisotropy of Composite Films and for In Situ Characterization of the Film Rheology. *Adv. Funct. Mater.* **26**, 3796–3808 (2016).
 29. Zaben, A., Kitenbergs, G. & Cēbers, A. 3D motion of flexible ferromagnetic filaments under a rotating magnetic field. *Soft Matter* **16**, 4477–4483 (2020).
 30. Tierno, P., Claret, J., Sagués, F. & Cābers, A. Overdamped dynamics of paramagnetic ellipsoids in a precessing magnetic field. *Phys. Rev. E - Stat. Nonlinear, Soft Matter Phys.* **79**, 1–6 (2009).
 31. Erb, R. M., Segmehl, J., Schaffner, M. & Studart, A. R. Temporal response of magnetically labeled platelets under dynamic magnetic fields. *Soft Matter* **9**, 498–505 (2013).
 32. Libanori, R., Erb, R. M. & Studart, A. R. Mechanics of platelet-reinforced composites assembled using mechanical and magnetic stimuli. *ACS Appl.*

- Mater. Interfaces* **5**, 10794–10805 (2013).
33. Hortense Le Ferrand, Bouville, F. & Studart, A. Design of textured multi-layered structures via magnetically assisted slip casting. *Soft Matter* 1–20 (2019) doi:10.1039/c9sm00390h.
 34. Le Ferrand, H. & Bouville, F. Processing of dense bioinspired ceramics with deliberate microstructure. *J. Am. Ceram. Soc.* **102**, 7253–7263 (2019).
 35. Le Ferrand, H. Modeling the effect of microstructure on elastic wave propagation in platelet-reinforced composites and ceramics. *Compos. Struct.* **224**, 111105 (2019).
 36. Garbin, A. *et al.* Acoustophoresis of disk-shaped microparticles: A numerical and experimental study of acoustic radiation forces and torques. *J. Acoust. Soc. Am.* **138**, 2759 (2015).
 37. Demirörs, A. F., Courty, D., Libanori, R. & Studart, A. R. Periodically microstructured composite films made by electric- and magnetic-directed colloidal assembly. *Proc. Natl. Acad. Sci. U. S. A.* **113**, 4623–4628 (2016).
 38. Yang, Z., Wei, J., Gizynski, K., Song, M. G. & Grzybowski, B. A. Interference-like patterns of static magnetic fields imprinted into polymer/nanoparticle composites. *Nat. Commun.* **8**, 1–8 (2017).
 39. Kokkinis, D., Schaffner, M. & Studart, A. R. Multimaterial magnetically assisted 3D printing of composite materials. *Nat. Commun.* **45**, 333–338 (2015).
 40. Martin, J. J., Fiore, B. E. & Erb, R. M. Designing bioinspired composite reinforcement architectures via 3D magnetic printing. *Nat. Commun.* **6**, 1–7 (2015).
 41. Camacho, J. M. & Sosa, V. alternative method to calculate the magnetic field

- of permanent magnets with azimuthal symmetry. *Rev. Mex. fisica E* **59**, 8–17 (2013).
42. Liu, G., Hou, S., Xu, X. & Xiao, W. Design of a new 1d halbach magnet array with good sinusoidal magnetic field by analyzing the curved surface. *Sensors* **21**, 1–17 (2021).
43. Schmied, J. U., Le Ferrand, H., Ermanni, P., Studart, A. R. & Arrieta, A. F. Programmable snapping composites with bio-inspired architecture. *Bioinspiration and Biomimetics* **12**, 026012 (2017).
44. Riley, K. S., Le Ferrand, H. & Arrieta, A. F. Modeling of snapping composite shells with magnetically aligned bio-inspired reinforcements. *Smart Mater. Struct.* **27**, 114003 (2018).
45. Zhang, J. & Wang, C. Study of rotation of ellipsoidal particles in combined simple shear flow and magnetic fields. *Proc. 2017 COMSOL Conf. Bost.* 1–6 (2017).
46. Lisjak, D. & Mertelj, A. Anisotropic magnetic nanoparticles: A review of their properties, syntheses and potential applications. *Prog. Mater. Sci.* **95**, 286–328 (2018).
47. Biswal, S. L. & Gast, A. P. Micromixing with linked chains of paramagnetic particles. *Anal. Chem.* **76**, 6448–6455 (2004).
48. Lee, K. M. & Son, H. Distributed multipole model for design of permanent-magnet-based actuators. *IEEE Trans. Magn.* **43**, 3904–3913 (2007).
49. Wahlstrom, N., Kok, M., Schon, T. & Gusafsson, F. Modeling magnetic fields using Gaussian processes. *IEEE* **1**, 3522–3526 (2013).
50. Behera, R. P., Muhammad, S. B. S., Jiaxuan, M. H. & Le Ferrand, H. Porous textured ceramics with controlled grain size and orientation. *J. Eur. Ceram.*

- Soc.* **41**, 617 (2021).
51. Schober, M., Dittmann, K., Gumbsch, P., Kuboki, T. & Hohe, J. Mechanical Microstructure Characterization of Discontinuous-Fiber Reinforced Composites by means of Experimental-Numerical Micro Tensile Tests. *Pamm* **19**, 2–3 (2019).
 52. Yanamandra, K., Chen, G. L., Xu, X., Mac, G. & Gupta, N. Reverse engineering of additive manufactured composite part by toolpath reconstruction using imaging and machine learning. *Compos. Sci. Technol.* **198**, 108318 (2020).
 53. Munaz, A., Shiddiky, M. J. A. & Nguyen, N. T. Recent advances and current challenges in magnetophoresis based micro magnetofluidics. *Biomicrofluidics* **12**, (2018).
 54. Lin, F. *et al.* Orientation Control of Graphene Flakes by Magnetic Field: Broad Device Applications of Macroscopically Aligned Graphene. *Adv. Mater.* **29**, 1–6 (2017).
 55. Erb, R. M., Libanori, R., Rothfuchs, N. & Studart, A. R. Composites reinforced in three dimensions by using low magnetic fields. *Science (80-.)*. **335**, 199–204 (2012).
 56. Yaraghi, N. A. & Kisailus, D. Biomimetic Structural Materials: Inspiration from Design and Assembly. *Annu. Rev. Phys. Chem.* **69**, 23–57 (2018).
 57. Le Ferrand, H. & Athanasiou, C. E. A Materials Perspective on the Design of Damage-Resilient Bone Implants Through Additive/Advanced Manufacturing. *Jom* **72**, 1195–1210 (2020).
 58. Ghazlan, A. *et al.* Inspiration from Nature’s body armours – A review of biological and bioinspired composites. *Compos. Part B Eng.* **205**, 108513

- (2021).
59. Abrougui, M. M., Srasra, E., Lopez-Lopez, M. T. & Duran, J. D. G. Rheology of magnetic colloids containing clusters of particle platelets and polymer nanofibres. *Philos. Trans. R. Soc. A Math. Phys. Eng. Sci.* **378**, 20190255 (2020).
 60. Wu, S. *et al.* Symmetry-Breaking Actuation Mechanism for Soft Robotics and Active Metamaterials. *ACS Appl. Mater. Interfaces* **11**, 41649–41658 (2019).
 61. Borin, D., Stepanov, G. & Dohmen, E. On anisotropic mechanical properties of heterogeneous magnetic polymeric composites. *Philos. Trans. R. Soc. A Math. Phys. Eng. Sci.* **377**, 20180212 (2019).
 62. Sydney Gladman, A., Matsumoto, E. A., Nuzzo, R. G., Mahadevan, L. & Lewis, J. A. Biomimetic 4D printing. *Nat. Mater.* **15**, 413–418 (2016).
 63. Ma, S. Q. *et al.* Recent progress in 4D printing of stimuli-responsive polymeric materials. *Sci. China Technol. Sci.* **63**, 532–544 (2020).
 64. Martin, J. J., Fiore, B. E. & Erb, R. M. Designing bioinspired composite reinforcement architectures via 3D magnetic printing. *Nat. Commun.* **6**, 1–7 (2015).
 65. Pereira, T., Leme, C. L. A. P., Marschner, S. & Rusinkiewicz, S. Printing anisotropic appearance with magnetic flakes. *ACM Trans. Graph.* **36**, 1–10 (2017).
 66. Huber, C. *et al.* Topology optimized and 3D printed polymer-bonded permanent magnets for a predefined external field. *J. Appl. Phys.* **122**, 053904 (2017).
 67. Huber, C. *et al.* 3D print of polymer bonded rare-earth magnets, and 3D magnetic field scanning with an end-user 3D printer. *Appl. Phys. Lett.* **109**,

162401 (2016).

68. Domingo-Roca, R., Jackson, J. C. & Windmill, J. F. C. 3D-printing polymer-based permanent magnets. *Mater. Des.* **153**, 120–128 (2018).